Revival dynamics in a traversable wormhole

Stephan Plugge,[1,*] Étienne Lantagne-Hurtubise,[1,†] and Marcel Franz[1]

[1] *Department of Physics and Astronomy & Quantum Matter Institute, University of British Columbia, Vancouver BC, Canada V6T 1Z4*

(Dated: March 10, 2020)

Quantum effects can stabilize wormhole solutions in general relativity, allowing information and matter to be transported between two connected spacetimes. Here we study the revival dynamics of signals sent between two weakly coupled quantum chaotic systems, represented as identical Sachdev-Ye-Kitaev models, that realize holographically a traversable wormhole in anti-de Sitter spacetime AdS_2 for large number N of particles. In this limit we find clear signatures of wormhole behavior: an excitation created in one system is quickly scrambled under its unitary dynamics, and is reassembled in the other system after a characteristic time consistent with holography predictions. This leads to revival oscillations that at low but finite temperature decay as a power-law in time. For small N we also observe revivals and show that they arise from a different, non-gravitational mechanism.

General relativity allows for wormhole solutions connecting two approximately flat space-times – the Einstein-Rosen bridge [1]. Unfortunately, such wormholes are known to be unstable and cannot be used to transmit matter or information. The ER bridge solution can be stabilized by the insertion of exotic matter with negative rest energy, but such matter is not available classically [2]. In a remarkable development, recent work in quantum gravity demonstrated that quantum effects can substitute for the exotic matter and stabilize a *traversable wormhole* [3–8]. From a practical standpoint it is unlikely that genuine quantum gravity effects, such as the traversable wormhole formation, can be probed experimentally in the foreseeable future. One can imagine, however, testing these effects in quantum systems that are related to gravity by holographic dualities – thus enabling, at least in principle, explorations of otherwise inaccessible physical phenomena in tabletop experiments.

An example of this duality, notable for its simplicity and wide appeal, is the Sachdev-Ye-Kitaev (SYK) model [9, 10], believed to be holographically dual to an extremal black hole embedded in AdS_2 [10–12]. The model shows extensive residual entropy, emergent (weakly broken) conformal invariance and is maximally chaotic [13], all properties shared with black holes. At the same time the SYK model is sufficiently simple to be analytically tractable in the limit of a large number N of particles. There now exist several proposed physical realizations of the SYK model and its variants in atomic and solid-state systems [14–19], making it a potential platform for laboratory studies of quantum dynamics of black holes.

In this Letter we study a pair of weakly coupled SYK models which, according to recent work by Maldacena and Qi [20], furnishes a holographic realization of an eternal traversable wormhole in AdS_2. The model exhibits many interesting properties [21–24] and its physical realization based on the proposed SYK platforms has been discussed [25]. It is defined by Hamiltonian

$$H = H_L^{\mathrm{SYK}} + H_R^{\mathrm{SYK}} + i\mu \sum_j \chi_L^j \chi_R^j \tag{1}$$

where H_α^{SYK} describe the SYK models

$$H_\alpha^{\mathrm{SYK}} = \sum_{i<j<k<l} J_{ijkl} \chi_\alpha^i \chi_\alpha^j \chi_\alpha^k \chi_\alpha^l \ , \tag{2}$$

and $\alpha = L, R$ refer to the "left" and "right" side of the wormhole. Each contains N Majorana operators respecting $(\chi_\alpha^j)^\dagger = \chi_\alpha^j$ and $\{\chi_\alpha^i, \chi_\beta^j\} = \delta^{ij}\delta_{\alpha\beta}$. The real-valued random couplings J_{ijkl} are drawn from a Gaussian distribution with $\overline{J_{ijkl}} = 0$, $\overline{J_{ijkl}^2} = \frac{3!J^2}{N^3}$ and are, crucially, identical for $\alpha = L, R$.

The Maldacena-Qi (MQ) model Eq. (1) is believed to be dual to a traversable wormhole for small coupling, $\mu \ll J$, and low temperatures $T < \mu$ [20]. The key property that makes it a wormhole is the following. Starting in the ground state $|\Psi_0\rangle$ of the model, imagine creating an excitation on the right side $\chi_R^j|\Psi_0\rangle$. In the absence of coupling ($\mu = 0$), the excitation will rapidly dissipate due to the chaotic nature of the SYK model [10, 12]. Quantum information contained in the excitation will be *scrambled* among the $2^{N/2}$ states comprising the Hilbert space of H_R^{SYK}, becoming effectively lost to all simple observables. Remarkably, when the two systems are coupled by a small μ, the scrambled excitation is instead transported to the left side where it is 'unscrambled' to its original form: after a characteristic time t_{re}, the state of the system becomes close to $\chi_L^j|\Psi_0\rangle$. In quantum gravity language, the particle has passed through the wormhole.

While this revival property has been predicted based on the gravity interpretation of the MQ model [20], a direct observation within the quantum mechanical description of Eqs. (1)-(2) is yet to be achieved. This is the main goal of the present work. To this end we employ two complementary approaches. First, numerical exact diagonalization (ED) of the Hamiltonian (1) yields the complete set of many-body eigenstates $|\Psi_n\rangle$ with energy E_n.

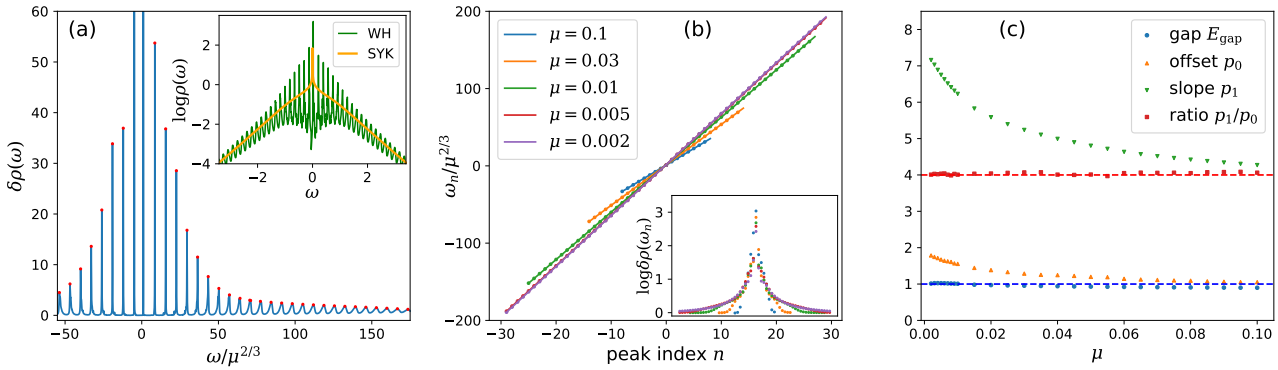

FIG. 1. Spectral features of the MQ model obtained from numerical solution of the SD equations (4) in real time and at small temperatures $T \ll \mu$. (a) inset: spectral functions for SYK (ρ_0, $\mu = 0$) and wormhole (ρ_+, $\mu = 0.004$). Main panel: relative spectral weight $\delta\rho(\omega) = \rho_+/\rho_0$. Red dots indicate positions of the dominant peaks analyzed further in (b,c). (b) peak location ω_n vs index n counted from the central peak ω_0 in (a). A linear fit $\omega_n = p_1 n + p_0$ is indicated. Inset: peak heights $\delta\rho(\omega_n)$ vs n, with $\delta\rho(\omega_n \gg 1) = 1$ reflecting the approach to SYK behavior at high energies. (c) spectral gap $E_{\rm gap} = \omega_0$, offset p_0 and slope p_1 of linear fits in (b), and ratio p_1/p_0 as a function of μ; $E_{\rm gap}$ and $p_{0,1}$ are in units $\mu^{2/3}$.

Any observable or correlation function can then be computed exactly; however, ED is limited to small systems with $2N \leq 32$. The second approach consists of solving the saddle-point equations for the averaged fermion propagator

$$G_{\alpha\beta}(\tau_1, \tau_2) = \frac{1}{N}\sum_j \langle \mathcal{T}\chi^j_\alpha(\tau_1)\chi^j_\beta(\tau_2)\rangle, \qquad (3)$$

where $\mathcal{T}$ denotes imaginary-time ordering and $\langle\cdots\rangle$ stands for thermal average. For the SYK model this approach is asymptotically exact in the limit of large N.

Large-N solution.– Under the assumption of time-translation invariance, $G_{\alpha\beta}(\tau_1, \tau_2) = G_{\alpha\beta}(\tau_1 - \tau_2)$, and the mirror symmetry between L and R systems which constrains $G_{RR}(\tau) = G_{LL}(\tau)$ and $G_{RL}(\tau) = -G_{LR}(\tau)$, the saddle-point equations of the MQ model can be reduced to a single pair of self-consistent equations [26],

$$G_+(i\omega_n) = [i\omega_n - \mu - \Sigma_+(i\omega_n)]^{-1}, \qquad (4)$$
$$\Sigma_+(\tau) = -\frac{1}{4}J^2\left[3G_+^2(\tau)G_+(-\tau) + G_+^3(-\tau)\right].$$

Here we defined $G_\pm(\tau) = G_{LL}(\tau) \pm iG_{LR}(\tau)$ and similar for the self energies $\Sigma_\pm(\tau)$ (henceforth, we set $J = 1$). The advantage of this representation is that the equations for G_+ and G_- decouple. Since the propagators are related by $G_\pm(\tau) = -G_\mp(-\tau)$, solving Eqs. (4) yields both $G_\pm$ and can be used to reconstruct the full $G_{\alpha\beta}(\tau)$.

To access dynamical properties of the MQ model, we switch to real-time representation of the SD equations in Eq. (4) and employ a weighted-iteration scheme [20, 25] to find self-consistent solutions (G, Σ) [26]. In the limit of weak coupling μ where wormhole effects are presumed to arise, it is necessary to employ both a large frequency cutoff $\omega_{\rm max} \gg J$ and small spacing $\delta\omega \ll \mu$ to resolve fine details of the spectral function *and* capture slowly decaying tails at high energies that are characteristic of SYK physics. This makes numerics challenging [27]. By implementing the symmetries in Eq. (4) we are able to go beyond earlier works [20, 21].

Spectral function.– In Fig. 1 we analyze the spectral function $\rho_+(\omega) = -\frac{1}{\pi}\mathrm{Im}G^{\rm ret}_+(\omega)$ of the MQ model obtained from the large-N saddle-point solution. A key observation in Fig. 1a is the series of evenly-spaced spectral peaks at frequencies ω_n shown in Fig. 1b. Holography predicts the emergence of two conformal "towers" of states at energies [20]

$$E_n^{\rm conf} = \epsilon\,(\Delta + n)\,, \quad E_n^{\rm bg} = \epsilon\sqrt{2(1-\Delta)}\left(n + \frac{1}{2}\right), \qquad (5)$$

where $\Delta = 1/4$ is the fermion scaling dimension. These towers correspond to conformal excitations and a "boundary graviton" in the gravity interpretation of the MQ model [20], respectively. From the SD equations (4) and scaling arguments one expects $\epsilon \sim \mu^{2/3}$, leading to a spectral gap $E_0^{\rm conf} \sim \Delta\mu^{2/3}$. Our approach in Fig. 1c hence is two-fold: We first extract $E_{\rm gap}$ from the lowest peak in the spectral function; then fit the remaining peak positions to a linear dependence $\omega_n \simeq p_1 n + p_0$ and extract the offset p_0 and slope p_1. We observe evenly-spaced peaks at all energies with $|n| \geq 1$, indicative of conformal behavior with fermion scaling dimension $\Delta \simeq p_0/p_1 = \frac{1}{4}$, assuming $\omega_n = E_n^{\rm conf}$ in Eq. (5). We find this ratio to be robust across *several decades* in μ [26]. Surprisingly, the offset p_0 does not match the dominant central peak $E_{\rm gap} \simeq \mu^{2/3}$ which appears to be an outlier, removed from the conformal tower of states. Further, we find no evidence for the "boundary graviton" states among the dominant peaks in $\rho_+(\omega)$ [28].

The full spectrum generated by Eqs. (4) comprises states encoded in both $\rho_+(\omega)$ and $\rho_-(\omega) = \rho_+(-\omega)$. For

clarity we excluded the latter in Fig. 1, but the implication is that we obtain two conformal towers related by reflection about $\omega = 0$. The peak spacing for spectral functions $\rho_{\alpha\beta}(\omega)$ then leads to $\Delta' = p_0'/p_1' \simeq \frac{1}{2}$.

Revival dynamics. – Revival dynamics are captured by the transmission amplitudes between the two systems

$$T_{\alpha\beta}(t) = 2|G^{>}_{\alpha\beta}(t)|\,,\; G^{>}_{\alpha\beta}(t) = \frac{\theta(t)}{N}\sum_j \langle \chi^j_\alpha(t)\chi^j_\beta(0)\rangle. \tag{6}$$

The transmission $T^2_{\alpha\beta}(t)$ then reflects the probability to recover $\chi^j_\alpha(t)$ after inserting $\chi^j_\beta(0)$ initially, averaged over all modes j.

In Fig. 2 we show $T_{\alpha\beta}(t)$ obtained from the numerical solution of the SD equations. For $\mu = 0$, we recover the usual SYK power-law $T_{\rm SYK}(t) = 2|G^{>}_{\rm SYK}(t)| \sim t^{-1/2}$. For small $\mu > 0$, $T_{LL}(t)$ initially follows closely the SYK result. Then, at time $t_{\rm re}$, a sharp peak in $T_{LR}(t)$ indicates that the excitation has traversed to the other side. The situation at $t = t_{\rm re}$ is similar to the initial configuration with L and R reversed – thus at $t = 2t_{\rm re}$ we expect a recurrence of the excitation at its original position, indicated by a peak at $T_{LL}(2t_{\rm re})$, and so on. As found in Fig. 2, the characteristic frequency $\omega_{\rm re} = \frac{p_1}{2\pi} \sim \mu^{2/3}$ for such oscillations is consistent with the prediction from holography [20, 26]. It is much larger than the naive guess $\omega_{\rm re} \sim \mu$, indicating that the chaotic SYK interactions assist the transmission of information between the two sides of the wormhole. For small μ the oscillations decay as a power-law in time with an exponent approaching $\frac{1}{2}$ [26], indicative of an SYK-like envelope to the revivals. This shows that the MQ model (at finite temperature) contains contributions beyond the gravitational picture, which predicts an *eternal* traversable wormhole where particles bounce back and forth indefinitely. Further the observed revivals can be contrasted with the large μ limit, which is not dual to a wormhole. A simple calculation gives $T_{\alpha\beta}(t) \equiv 1$ in the ground state of the system for $\mu \gg 1$, which is reflected in the suppressed oscillation amplitudes for large μ, cf. Fig. 2.

Note that the Fourier transform of the transmission, $F_{\alpha\beta}(\omega) = \int dt e^{i\omega t} T^2_{\alpha\beta}(t)$, can be written as a spectral auto-correlation function [26]

$$F_{\alpha\beta}(\omega) = \frac{2}{\pi}\int_0^\infty d\omega' \rho_{\alpha\beta}(\omega')\rho_{\alpha\beta}(\omega' + |\omega|). \tag{7}$$

Sharp revivals thus rely on a series of evenly-spaced peaks in $F_{\alpha\beta}(\omega)$, originating from strong peak-spacing correlations in the spectral functions $\rho_{\alpha\beta}(\omega)$, cf. Fig. 1. The "beating" in Fig. 2 stems from the shift of the lowest spectral peak. The transmission does not decay to zero between peaks – this finite value persists up to times of order inverse temperature β, which sets the width of the $\omega = 0$ peak in $F_{\alpha\beta}(\omega)$ [26]. At long times $t > \beta$ the system eventually thermalizes, $T_{\alpha\beta}(t) \to 0$, losing any memory of the initial excitation.

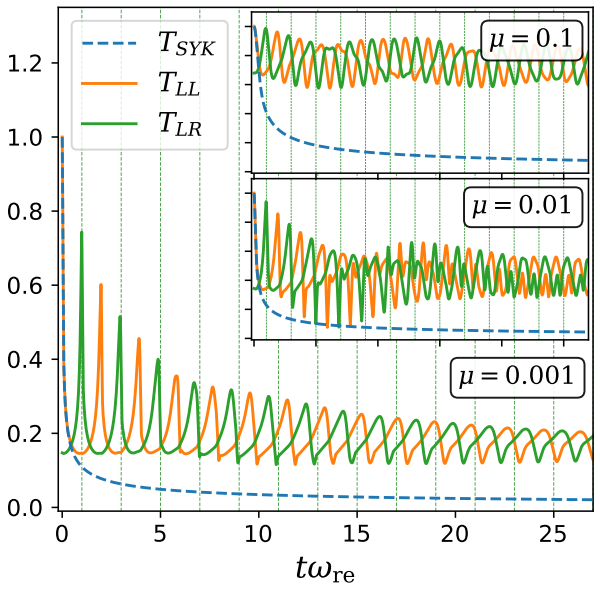

FIG. 2. Revival dynamics in transmission amplitudes $T_{LL,LR}$ in Eq. (6); $T_{\rm SYK} = T_{LL}(\mu = 0)$ refers to an uncoupled SYK model. Main panel and insets show data for various μ, with time axes rescaled by $\omega_{\rm re} = p_1/2\pi$, cf. Fig. 1. Vertical lines indicate times $t_{{\rm re},n} = (2n+1)/\omega_{\rm re}$ for which an excitation $\chi_R(0)$ is expected to re-assemble on the left side.

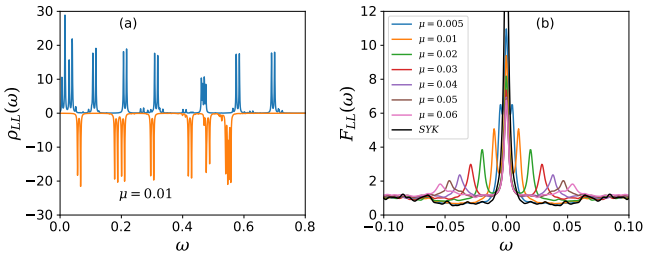

FIG. 3. Spectral properties of the MQ model from exact diagonalization for $2N = 16$ Majorana fermions. (a) spectral function ρ_{LL} for two distinct disorder realizations, showing doublets of states split by ω_D. (b) Auto-correlation $F_{LL}(\omega)$ for various μ, each averaged over 50 disorder realizations.

Spectrum from ED.– The corresponding ED results for the spectral function $\rho_{LL}(\omega)$ are shown in Fig. 3. We here find no evidence for a conformal tower of states, presumably due to finite-N effects. Instead, for $\mu \ll 1$ the spectral function consists of a collection of doublets separated by a splitting ω_D. The position of these doublets in energy is uncorrelated between different disorder realizations, see Fig. 3a. As a result, averaging the spectral function does not produce the spectral peaks expected from the large-N solution. However, averaging the spectral auto-correlation function $F_{\alpha\beta}(\omega)$ [Eq. (7)] retains a clear signal at the doublet splitting frequency ω_D, while high-frequency components are washed out and roughly follow the SYK continuum, see Fig. 3b.

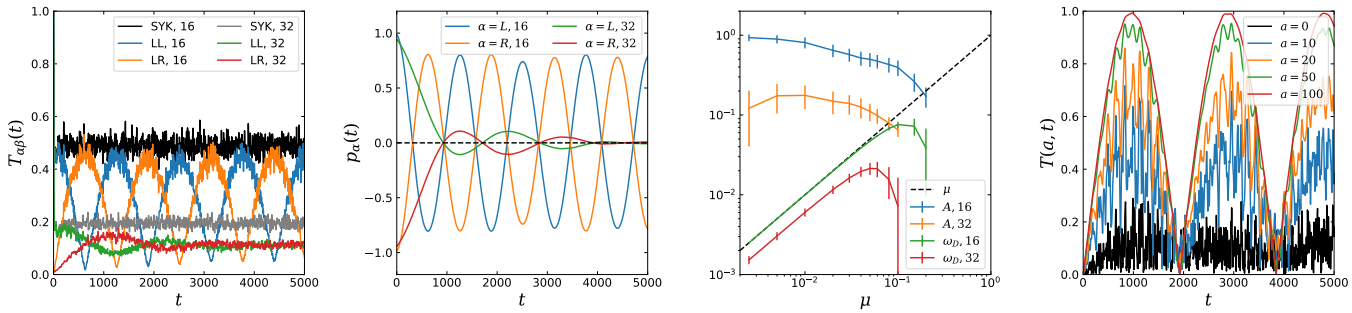

FIG. 4. Revival dynamics from ED with $\mu = 0.005$. (a) Transmission amplitudes $T_{\alpha\beta}(t)$ for $2N = 16, 32$ averaged over 50 disorder realizations. The SYK result ($\mu = 0$) is plotted for reference. (b) Corresponding fermion parity oscillations $p_\alpha(t)$. (c) Scaling of the oscillation frequency ω_D and amplitude A of the parity oscillations in (b) as function of μ. The error bars represent the standard deviation computed from 50 disorder realizations. (d) Transmission amplitude $T(a,t)$ of low-energy states $|\psi_a\rangle$ [Eq. (8)], for $2N = 32$ and a single disorder realization.

Revival dynamics in ED.– Fig. 4 shows transmission amplitudes $T_{\alpha\beta}(t)$ for system sizes $2N = 16$ and 32 [29]. For a single disorder realization, we observe rapid oscillations modulated by a much slower envelope. The fast dynamics originate from the discreteness of the spectrum in ED ($\lambda \sim Ne^{-N}$ is the typical level spacing) and vary strongly between disorder realizations. Averaging $T_{\alpha\beta}(t)$ over disorder smooths them out and retains only the envelope, see Fig. 4a. Note that the oscillations are less peaked than in large-N, since $F_{\alpha\beta}(\omega)$ shows a single peak at frequency ω_D rather than a series of evenly-spaced peaks. The frequency ω_D of the envelope is precisely the doublet splitting identified in Fig. 3. It scales linearly with μ for $\mu < \lambda$ and sub-linearly for $\lambda < \mu \ll 1$, see Fig. 4c. The latter is the regime of interest for the wormhole solution – however, a power-law $\omega_D \sim \mu^{2/3}$, as predicted by scaling arguments [20] and obtained in SD numerics, cannot be extracted from ED.

A cleaner way to observe the revival oscillations is from the time evolution of *fermionic parities* on each side, $p_\alpha(t) = \langle\Psi|P_\alpha(t)|\Psi\rangle$ with $P_\alpha = (-i)^{N/2}\prod_k \chi_\alpha^k$ and the initial excitation $|\Psi\rangle = \chi_R^j|\Psi_0\rangle$. This observable tracks the propagation of fermion modes between the two sides regardless of the precise quantum state, and thus is less sensitive to disorder, as shown in Fig. 4b.

Contrary to the expectation that ED should approach the saddle-point results as N increases, the amplitude of oscillations in $T_{\alpha\beta}(t)$ and $p_\alpha(t)$ actually goes *down* significantly when increasing $2N$ from 16 to 32 (see Fig. 4a-c). This is because conformal towers of states are absent for small N. The observed revivals in ED do not rely on a series of evenly-spaced spectral peaks, but rather on a series of spectral doublets with roughly the same splitting, as shown in Fig. 3. When N increases the distribution of doublet splitting frequencies become wider [26], leading to a reduced oscillation amplitude. We also find an exact result for the averaged revivals in the $\mu \ll \lambda$ limit, valid only for $2N = 16$, which explains the corresponding absence of decay in Fig. 4a-b [26]. For the same reason, transmissions are improved drastically when considering *low-energy* excitations initially localized on one side. These can be generated by applying the projection

$$|\psi^j_{\alpha,a}\rangle = \frac{1}{\sqrt{C}}\sum_n e^{-\frac{a(E_n-E_0)}{|E_0|}}|n\rangle\langle n|\chi^j_\alpha|0\rangle, \qquad (8)$$

with normalization C. For $a > 0$ this shifts the spectral weight of the excitation to a few low-energy doublets of states. As a result the transmissions $T_a(t) = |\langle\psi^j_{L,a}(t)|\psi^j_{R,a}\rangle|$ show oscillations with an amplitude that increases with a and saturates at $T_a(t_{\rm tr}) \sim 1$, see Fig. 4d.

Discussion and outlook.– We studied dynamical properties of the Maldacena-Qi model, believed to be holographically dual to a traversable wormhole. In the large-N limit, sharp revival oscillations at frequency $\sim \mu^{2/3}$ are observed in fermion transmission amplitudes, consistent with predictions of quantum gravity. The revivals arise from *two* conformal towers of states that emerge from the SYK continuum, and for weak couplings μ their amplitude decays as a power-law in time. For small N, no towers of states are visible in exact diagonalization. Revivals instead rely on a series of approximately equal-split doublets, and the revival amplitude *decreases* with N. Only *low-energy* states localized in one system can be transmitted with probability ~ 1. The associated fermion parity oscillations could provide an experimental probe of revivals in the proposed platforms for physical realization [25], by employing parity measurements after "severing" the wormhole (quench to $\mu = 0$).

Our work leaves several interesting open questions that are relevant to future experimental explorations of revivals in coupled SYK models. How do the dynamics of the MQ model change with increasing N, from being dominated by finite-size effects to arising from conformal behavior? In other words, how does the dual gravitational description emerge in a system with finite N? These questions are out of reach of exact diagonalization, but progress could be made with Krylov subspace

methods, recently used to study quantum chaos in the SYK model [30]. Another interesting avenue would be to relate the present results to circuit-based teleportation protocols using traversable wormholes [31, 32].

Note: After completion of this work, we learned about a related parallel study by X.-L. Qi and P. Zhang that focuses on finite-temperature effects in the MQ model [33].

Acknowledgements.– We thank O. Can, B. Kobrin, J. Maldacena, M. Rozali, X.-L. Qi, and S. Sahoo for useful discussions. This research was supported by SBQMI at UBC, UBC ARC Sockeye computational facilities, NSERC, and CIfAR. Further, E.L.H. acknowledges support from the Heising-Simons Foundation, the Simons Foundation, and National Science Foundation Grant No. NSF PHY-1748958 at KITP.

* plugge@phas.ubc.ca
† lantagne@phas.ubc.ca

[1] A. Einstein and N. Rosen, "The particle problem in the general theory of relativity," Phys. Rev. **48**, 73–77 (1935).
[2] Michael S. Morris and Kip S. Thorne, "Wormholes in spacetime and their use for interstellar travel: A tool for teaching general relativity," Am. J. Phys. **56**, 395–412 (1988).
[3] P. Gao, D. L. Jafferis, and A. C. Wall, "Traversable wormholes via a double trace deformation," J. High Energy Phys. **12**, 151 (2017).
[4] Juan Maldacena, Douglas Stanford, and Zhenbin Yang, "Diving into traversable wormholes," Fortschr. Phys. **65**, 1700034 (2017).
[5] Juan Maldacena, Alexey Milekhin, and Fedor Popov, "Traversable wormholes in four dimensions," arXiv:1807.04726 (2018).
[6] Dongsu Bak, Chanju Kim, and Sang-Heon Yi, "Bulk view of teleportation and traversable wormholes," J. High Energy Phys. **2018**, 140 (2018).
[7] Ping Gao and Hong Liu, "Regenesis and quantum traversable wormholes," J. High Energy Phys. **2019**, 48 (2019).
[8] Zicao Fu, Brianna Grado-White, and Donald Marolf, "Traversable asymptotically flat wormholes with short transit times," Classical and Quantum Gravity **36**, 245018 (2019).
[9] Subir Sachdev and Jinwu Ye, "Gapless spin-fluid ground state in a random quantum heisenberg magnet," Phys. Rev. Lett. **70**, 3339 (1993).
[10] A. Kitaev, "A simple model of quantum holography," in KITP Strings Seminar and Entanglement 2015 Program (2015).
[11] Subir Sachdev, "Bekenstein-hawking entropy and strange metals," Phys. Rev. X **5**, 041025 (2015).
[12] Juan Maldacena and Douglas Stanford, "Remarks on the sachdev-ye-kitaev model," Phys. Rev. D **94**, 106002 (2016).
[13] Juan Maldacena, Stephen H. Shenker, and Douglas Stanford, "A bound on chaos," J. High Energy Phys. **2016**, 106 (2016).
[14] Ippei Danshita, Masanori Hanada, and Masaki Tezuka, "Creating and probing the sachdevyekitaev model with ultracold gases: Towards experimental studies of quantum gravity," Prog. Theor. Exp. Phys. **2017**, 083I01 (2017).
[15] D. I. Pikulin and M. Franz, "Black hole on a chip: Proposal for a physical realization of the sachdev-ye-kitaev model in a solid-state system," Phys. Rev. X **7**, 031006 (2017).
[16] Aaron Chew, Andrew Essin, and Jason Alicea, "Approximating the sachdev-ye-kitaev model with majorana wires," Phys. Rev. B **96**, 121119(R) (2017).
[17] Anffany Chen, R. Ilan, F. de Juan, D. I. Pikulin, and M. Franz, "Quantum holography in a graphene flake with an irregular boundary," Phys. Rev. Lett. **121**, 036403 (2018).
[18] Marcel Franz and Moshe Rozali, "Mimicking black hole event horizons in atomic and solid-state systems," Nat. Rev. Mater. **3**, 491 (2018).
[19] Alexander Altland, Dmitry Bagrets, and Alex Kamenev, "Sachdev-ye-kitaev non-fermi-liquid correlations in nanoscopic quantum transport," Phys. Rev. Lett. **123**, 226801 (2019).
[20] Juan Maldacena and Xiao-Liang Qi, "Eternal traversable wormhole," arXiv:1804.00491 (2018).
[21] Antonio M. García-García, Tomoki Nosaka, Dario Rosa, and Jacobus J. M. Verbaarschot, "Quantum chaos transition in a two-site sachdev-ye-kitaev model dual to an eternal traversable wormhole," Phys. Rev. D **100**, 026002 (2019).
[22] Juan Maldacena and Alexey Milekhin, "SYK wormhole formation in real time," arXiv:1912.03276 .
[23] Yiming Chen and Pengfei Zhang, "Entanglement entropy of two coupled syk models and eternal traversable wormhole," J. High Energy Phys. **2019**, 33 (2019).
[24] Fabien Alet, Masanori Hanada, Antal Jevicki, and Cheng Peng, "Entanglement and Confinement in Coupled Quantum Systems," arXiv:2001.03158 .
[25] Étienne Lantagne-Hurtubise, Stephan Plugge, Oguzhan Can, and Marcel Franz, "Diagnosing quantum chaos in many-body systems using entanglement as a resource," Phys. Rev. Research **2**, 013254 (2020).
[26] For further discussion, additional data and analysis, see the supplementary material available at [online link].
[27] In order to observe revivals, it is crucial to extract more than just an energy gap from saddle-point equations or exact diagonalization. A single-scale expression $G_{LL}(\tau) \sim e^{-E_{\rm gap}\tau} \rightarrow G_{LL}(t) \sim e^{-iE_{\rm gap}t}$ [20, 21] does *not* predict revivals, cf. Eqs. (6). In imaginary-time formulation, revivals associated with higher energy scales (conformal tower) are hidden in the early-time, non-exponential transient behavior of $G_{LL}(\tau)$.
[28] The spectral function shows additional subdominant peaks which might be related to the boundary graviton tower. However, due to their small amplitude and rapid decay at large ω we were unable to establish their identity conclusively.
[29] We consider the simplest case N mod 8 = 0, corresponding to the Gaussian orthogonal ensemble (GOE) in the random matrix theory classification for a single SYK model. We thus avoid spectral degeneracies present for the unitary (GUE) and symplectic (GSE) ensembles which complicate the analysis.
[30] Bryce Kobrin, Zhenbin Yang, Gregory D Kahanamoku-Meyer, Christopher T Olund, Joel E Moore, Douglas

Stanford, and Norman Y Yao, "Many-body chaos in the sachdev-ye-kitaev model," arXiv:2002.05725 (2020).

[31] Adam R. Brown, Hrant Gharibyan, Stefan Leichenauer, Henry W. Lin, Sepehr Nezami, Grant Salton, Leonard Susskind, Brian Swingle, and Michael Walter, "Quantum Gravity in the Lab: Teleportation by Size and Traversable Wormholes," arXiv:2002.05725 (2019).

[32] Ping Gao and Daniel Louis Jafferis, "A Traversable Wormhole Teleportation Protocol in the SYK Model," arXiv:1911.07416 (2019).

[33] Xiaoliang Qi and Pengfei Zhang, "The Coupled SYK model at Finite Temperature," arXiv (2020).

[34] Sumilan Banerjee and Ehud Altman, "Solvable model for a dynamical quantum phase transition from fast to slow scrambling," Phys. Rev. B **95**, 134302 (2017).

SUPPLEMENTARY MATERIAL

Large-N saddle point equations

The derivation of the large-N saddle point equations for the problem defined by Eqs. (1)-(2) in the main text proceeds along the same lines as for the original SYK model [S10, S12], so we only outline the key steps here and focus on the novel features that arise from having two coupled SYK models. The first step is to reformulate the theory using an imaginary-time path integral with Majorana fields represented as anticommuting Grassmann variables. Averaging over the quenched disorder in coupling constants J_{ijkl} then leads to an action for averaged propagators $G_{\alpha\beta}(\tau_1,\tau_2)$ defined by Eq. (3). The resulting action is quadratic in the fermion fields and, when these are integrated out, has the following form [S20, S25]

$$S=-N\ln\mathrm{Pf}(\delta_{\alpha\beta}\partial_\tau-\Sigma_{\alpha\beta})+\frac{N}{2}\int_{\tau_1,\tau_2}\sum_{\alpha,\beta}\left[\Big(\Sigma_{\alpha\beta}(\tau_1,\tau_2)-\mu\sigma^y_{\alpha\beta}\delta(\tau_1-\tau_2)\Big)G_{\alpha\beta}(\tau_1,\tau_2)-\frac{J^2}{4}G_{\alpha\beta}(\tau_1,\tau_2)^4\right], \quad \text{(S1)}$$

where σ^y is a Pauli matrix acting in the LR space. The Lagrange multiplier $\Sigma_{\alpha\beta}$ has been introduced to enforce Eq. (3) and can be interpreted as the fermion self-energy. For $\mu=0$ the action (S1) describes two decoupled SYK models [S10, S12]. The large-N saddle-point equations are obtained by varying the action with respect to $\Sigma_{\alpha\beta}$ and $G_{\alpha\beta}$,

$$G_{\alpha\beta}(i\omega_n)=\left[i\omega_n-\mu\sigma^y-\Sigma(i\omega_n)\right]^{-1}|_{\alpha\beta}, \quad \text{(S2)}$$
$$\Sigma_{\alpha\beta}(\tau)=J^2G_{\alpha\beta}(\tau)^3, \quad \text{(S3)}$$

and $\omega_n=\pi T(2n+1)$ is the nth Matsubara frequency.

The solution of the saddle-point equations can be considerably simplified by exploiting symmetries. First, we notice that the MQ Hamiltonian is invariant under the exchange $\chi^j_L\to\chi^j_R$ and $\chi^j_R\to-\chi^j_L$ which implies $G_{LL}(\tau)=G_{RR}(\tau)$ and $G_{LR}(\tau)=-G_{RL}(\tau)$. The full matrix propagator can be therefore expressed in terms of its two independent components as

$$G(\tau)=G_{LL}(\tau)+i\sigma^yG_{LR}(\tau). \quad \text{(S4)}$$

To further simplify the solution it is useful to rotate into a new basis in the LR space by defining

$$G_\pm(\tau)=G_{LL}(\tau)\pm iG_{LR}(\tau), \quad \text{(S5)}$$
$$\Sigma_\pm(\tau)=\Sigma_{LL}(\tau)\pm i\Sigma_{LR}(\tau).$$

In the absence of interactions, that is when $J=0$, this rotation diagonalizes Eq. (S2) which is then solved by $G^0_\pm(i\omega_n)=1/(i\omega_n\mp\mu)$. Fourier transforming into the imaginary time domain one immediately obtains the second useful symmetry property

$$G^0_\mp(\tau)=-G^0_\pm(-\tau). \quad \text{(S6)}$$

In the new basis, Eq. (S3) can be rewritten as

$$\Sigma_\pm(\tau)=\frac{J^2}{4}\left[3G^2_\pm(\tau)G_\mp(\tau)+G^3_\mp(\tau)\right]. \quad \text{(S7)}$$

If we assume for a moment that symmetry (S6) is the property of the full interacting propagator then Eq. (S7) implies the same symmetry for the self energy, i.e. $\Sigma_\mp(\tau)=-\Sigma_\pm(-\tau)$. Therefore, we conclude that the symmetry (S6) of the non-interacting system is respected by the saddle-point equations in the presence of interactions. We can then substitute $G_\mp(\tau)=-G_\pm(-\tau)$ in Eq. (S7) which makes the equations for the + and − channel decouple, and leads to Eq. (4) of the main text.

Real-time and -frequency formulation of SD equations

To access transmission amplitudes or spectral features in real time and frequency, we analytically continue the final set of Schwinger-Dyson (SD) equations, Eq. (4) of the main text, following the procedures outlined in Refs. [S25, S34]. For completeness and to keep this work self-contained, we here outline the essential steps leading to the final set of real-time SD equations that we then solve numerically. Analytic continuation of Eq. (4) gives

$$G^{\mathrm{ret}}_+(\omega)=\left[\omega+i\eta-\mu-\Sigma^{\mathrm{ret}}_+(\omega)\right]^{-1},$$

with bare GF $G^0_+(\omega)=1/(\omega+i\eta-\mu)$ giving a Lorentzian peak (δ-function) in the spectral function at $\omega=\mu$. A tractable route to obtaining the retarded self-energy $\Sigma^{\mathrm{ret}}_+(\omega)$ consists of Fourier transforming the imaginary-time self-energy, going over to spectral representation of Matsubara Greens functions, and finally continuing to real frequency, using steps and identities outlined in Refs. [S25, S34]. This can either be done in LL-LR basis, afterwards adding up contributions according to Eq. (S5), or by directly operating on the decoupled SD equations for ± channels, given by Eq. (4). In both cases, for representation purposes, it is useful to retain the occupation functions of the LL,LR channels given by [S25]

$$n_{LL/LR}(t)=\int_{-\infty}^{\infty}d\omega\rho_{LL/LR}(\omega)n_F(\omega)e^{-i\omega t}, \quad \text{(S8)}$$

comprising even and odd frequency-parity combinations $\rho_{LL/LR}(\omega)=\frac{1}{2}[\rho_+(\omega)\pm\rho_+(-\omega)]$ of the spectral func-

tion $\rho_+(\omega) = -\frac{1}{\pi}\mathrm{Im}G^{\mathrm{ret}}_+(\omega)$, cf. Eq. (S5), and the Fermi function $n_F(\omega)$. The latter arises after carrying out Matsubara sums that transform imaginary to real frequencies in the spectral representation of GFs. In doing this we use various identities [S25] to relate Fermi/Bose occupation functions on frequency differences to products of individual Fermi functions, and finally find the retarded self-energy

$$\Sigma^{\mathrm{ret}}_+(\omega) = -2iJ^2\int_0^\infty dt e^{i(\omega+i\eta)t}\times \left[\mathrm{Re}[n^3_{LL}(t)] - i\mathrm{Im}[n^3_{LR}(t)]\right] . \tag{S9}$$

From here, to find a solution of the SD equations, we perform weighted numerical iterations [S12, S20, S25] transforming between time and frequency representations to evaluate self-energies and Dyson equations. We declare convergence to a physical solution once propagators and spectral functions stop changing within the accessible numerical resolution. For the results presented in this work, we employ a frequency cutoff $\omega_{\mathrm{max}} = 2^{11}$ with $N_{\mathrm{grid}} = 2^{28} - 2^{29}$ grid points for Fourier transforms and the SD iteration. For the smallest μ we consider, this leads to frequency spacings $\delta\omega \lesssim 10T \lesssim 100\mu$.

Generalization to order-q SYK-interactions

Similar simplifications as above are possible for generalized interactions with $q > 4$ SYK fermions [S12, S20] in Eq. (2) of the main text. Here we find self-energies

$$\Sigma^q_{\alpha\beta}(\tau) = J^2 G_{\alpha\beta}(\tau)^{q-1}, \tag{S10}$$

in place of Eq. (S3). The SD equations can be simplified in an analogous manner. We again switch to combinations $G_\pm(\tau)$ and find by the same steps as above

$$\Sigma^q_+(\tau) = \frac{J^2}{2^{q-1}}\{[G_+(\tau) - G_+(-\tau)]^{q-1} - [G_+(\tau) + G_+(-\tau)]^{q-1}\}. \tag{S11}$$

This is the generalization of Eqs. (4),(S7) to arbitrary q. With regards to the analytic continuation to real time and frequency, while intermediate steps are somewhat more tedious for general q (more Matsubara sums and Bose/Fermi function identities), by analogous steps one finds for the retarded self-energy

$$\Sigma^{\mathrm{ret},q}_+(\omega) = -2iJ^2\int_0^\infty dt e^{i(\omega+i\eta)t}\times \left[\mathrm{Re}[n^{q-1}_{LL}(t)] - i(-1)^{q/2}\mathrm{Im}[n^{q-1}_{LR}(t)]\right] . \tag{S12}$$

Here we again used $n_{LL/LR}(t) = \frac{1}{2}(n_+ \pm n_-)$ with time-dependent occupation $n_\pm(t) = \int d\omega \rho_+(\pm\omega) n_F(\omega) e^{-i\omega t}$, cf. Eq. (S8). This result allows to solve real-time and -frequency SD equations for the MQ model at arbitrary q in a unified manner. However note that by virtue of Eq. (S12), larger q leads to stronger non-linearity of the self-energy, implying more difficulty in ensuring numerical stability and convergence. Indeed upon numerically implementing the above equations for $q = 6$ or $q = 8$, by naive comparison to the simplest $q = 4$ case, we found the quality of solutions to deteriorate rapidly.

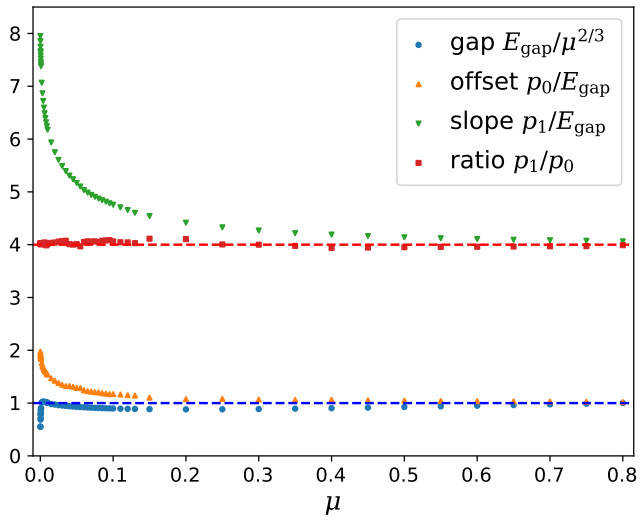

FIG. S1. Additional figure for spectral function analysis. The spectral gap stays remarkably close to $E_{\mathrm{gap}} \sim \mu^{2/3}$ for $\mu \in [10^{-4}, 0.8]$, over almost four orders of magnitude; deviations are observed at $\mu \lesssim 0.001$. Offsets and slopes of spectral peak series are plotted by dividing out E_{gap}, showing a divergence towards $\mu = 0$. This is even though both $p_{0,1}$ exhibit a down-turn similar to the gap when plotted in units $\mu^{2/3}$. The ratio of slope and offset, indicative of scaling dimension Δ, is robust at $\Delta^{-1} = p_1/p_0 \simeq 4$ over the full range of μ.

Extended data for spectral function analysis

Here we discuss additional results for the peak structure in the spectral function. As shown in Fig. S1, our results of Fig. 1 in the main text extend to a range of couplings $\mu \in [10^{-4}, 0.8]$ of almost four decades. The ratio of peak spacing slope to the offset, $\Delta^{-1} = p_1/p_0$, indicative of the fermion scaling dimension Δ of the presumed conformal tower of eigenstates in the spectral function, is remarkably robust over the full range of μ.

We also note a downturn of the spectral gap away from the conformal scaling prediction $E_{\mathrm{gap}} \simeq \mu^{2/3}J^{1/3}$, around $\mu \lesssim 0.001$. This is likely due to convergence problems for large separations of energy scales μ and $J = 1$. Recall that SYK spectral functions decay slowly, as power laws $\rho_{\mathrm{SYK}} \sim \omega^{-1/2}$, necessitating large cutoffs in numerical solutions of Schwinger-Dyson equations [S12]. In the wormhole case this goes along with a simultaneous need for high frequency resolution, to capture low-energy

physics on scales below μ [S20, S21, S25]. Similar to the spectral gap, the peak spacing slopes and offsets experience down-turn upon approaching $\mu \to 0$ (in units $\mu^{2/3}$, cf. Fig. 1 main text). After dividing out the diminishing gap $E_{\rm gap}$, cf. Fig. S1, one observes a systematic divergence of $p_{0,1}/E_{\rm gap}$ towards vanishing μ. In our numerics, relative scales thus seem more robust to finite resolution and cutoff than the absolute values of the gap etc.

Link between revival dynamics and spectral features

Revival dynamics are related to peaks in the spectral function in a subtle way. This is seen by considering transmissions, i.e. the square of transmission amplitudes $|T_{\alpha\beta}|^2 = 4G^{>}_{\alpha\beta}(t)[G^{>}_{\alpha\beta}(t)]^*$. After performing Fourier transforms and representing greater GFs via spectral functions according to

$$iG^{>}_{\alpha\beta}(\omega) = [1 - n_F(\omega)]\rho_{\alpha\beta}(\omega), \tag{S13}$$

these can be expressed (at zero temperature) as

$$\begin{aligned} F_{\alpha\beta}(\omega) &= \int d\omega e^{i\omega t}|T_{\alpha\beta}(t)|^2 \\ &= \frac{2}{\pi}\int_0^\infty d\omega' \rho_{\alpha\beta}(\omega')\rho_{\alpha\beta}(\omega'+|\omega|)\ . \end{aligned} \tag{S14}$$

Thus the positive-frequency auto-correlation of the spectral function gives the Fourier transform of revival dynamics. The equal energy spacings of spectral peaks (i.e., the conformal tower) obtained in the large-N solution for the spectral function $\rho_{\alpha\beta}(\omega)$ (Fig. 1 of the main text) obviously give rise to sharp features in auto-correlations at multiples of the energy spacing. As seen in Fig. S2, aside from a dominant peak at zero frequency, the most prominent feature is found at about twice the spectral gap $E_{\rm gap}$ in Fig. S1. Further we observe a series of spectral peaks in $F_{\alpha\beta}$, with an even-odd structure inherited from the spectral function, most clearly apparent in the plot of F_{LR} in Fig. S2. From here, we can associate the revival oscillations in transmission amplitudes to the (almost) equally-spaced peak series in $F_{\alpha\beta}$, with slight deviations from perfectly even spacings leading to the beating observed in Fig. 3 of the main text and Figs. S3 in the SM.

Thermalization and decay of revivals

Using the link between the spectral auto-correlation function and the revival dynamics, we now discuss two features of the revivals arising in the large-N solution: (*i*) thermalization of the system – that is, whether the auto-correlation function $T_{LL}(t) = |G^{>}_{LL}(t)| \to 0$ in the infinite-time limit (does the system retain memory of its initial state?), and (*ii*) the decay of revival oscillations (is the wormhole eternal?).

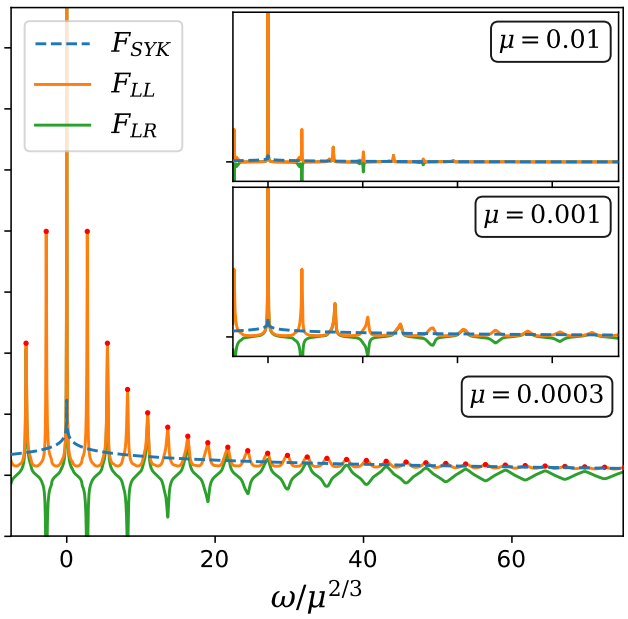

FIG. S2. Fourier transforms of the transmissions, obtained from the auto-correlation of spectral functions, cf. discussion in text and Eq. (S14). F_{LL} and F_{LR} show a distinct peak structure that is altogether absent from $F_{\rm SYK}$, aside from a default central peak at zero frequency. In the revival oscillations of Fig. 3 in main text, slight shifts of the peak frequencies observed here translate to a slow "beating" of oscillations.

The first question is related to the zero-frequency peak in $F_{LL}(\omega)$. We find that for temperatures $T \ll \mu \ll J$ it has a Lorentzian-like shape, with a width that is independent of μ but scales as $\Gamma \sim T$. Thus its Fourier transform contributes $\sim e^{-\Gamma t}$ to the transmission amplitude, with decay rate Γ. The system hence eventually thermalizes, on a timescale T^{-1} that is much longer than both J^{-1} (the timescale for the initial decay of two-point functions) and $\mu^{-2/3}$ (the timescale of revival oscillations). In the zero-temperature limit the system thus may fail to thermalize: a finite, constant value corresponding to the weight in the $\omega = 0$ peak remains up to infinite time.

The second question is more subtle, and requires understanding the structure of finite-frequency peaks in $F(\omega)$. For $T \ll \mu \ll J$ those peaks are roughly equally spaced, $\omega'_n = pn$, and resemble Lorentzians with a linearly-increasing width $\Gamma_n = \Gamma_0 n$. For the spectral auto-correlation function at low frequencies, we thus make the ansatz

$$F_{LL}(\omega) \approx \sum_n \frac{\Gamma_0 n}{(\omega - pn)^2 + (\Gamma_0 n)^2} \tag{S15}$$

Fourier transforming to real time, we obtain

$$T_{LL}(t)^2 = \int \frac{d\omega}{2\pi} F_{LL}(\omega) \approx 2\sum_{n>0} \cos(2\pi pnt)\, e^{-2\pi\Gamma_0 nt} \tag{S16}$$

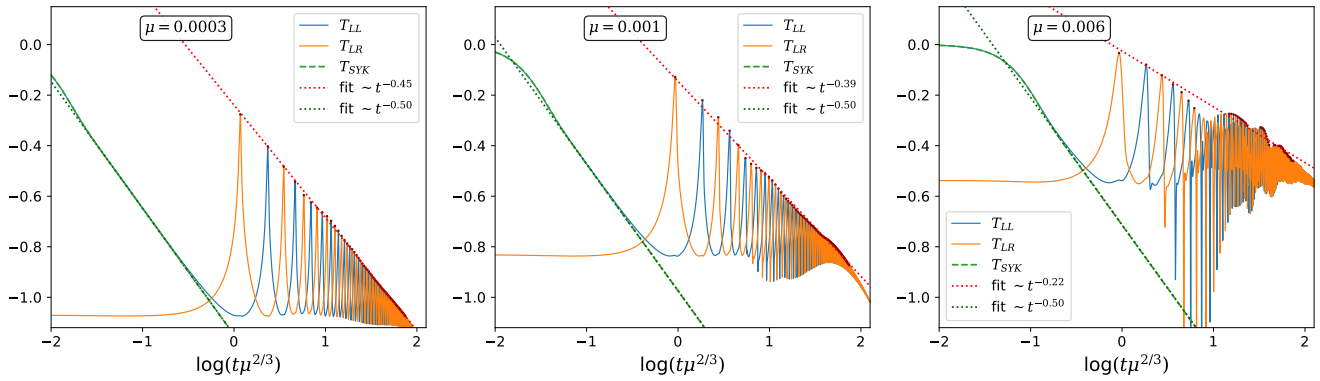

FIG. S3. Detailed transmission amplitude analysis of revival oscillations at large N, cf. Fig. 3 of the main text. We here focus on small $\mu = 0.0003,\ 0.001,\ 0.006$ as indicated in the figure panels, where "beating" effects are reduced and relatively clean revival oscillations can be observed. In each panel, we indicate and fit the decay of the SYK transmission amplitude $T_{\rm SYK}$ (unchanged, modulo shift on x-axis), as well as the revival peak heights. The revival peaks used for fitting of the revival amplitude decay are indicated by red dots, and fits are shown as dotted lines.

Whenever $t = t_{\rm re} = m/p$ with m integer, all oscillating terms interfere constructively, leading to a sharp revival signal. The height of this revival peak is then given by

$$T_{LL}(t_{\rm re})^2 \approx 2\sum_{n>0} e^{-2\pi\Gamma_0 nt} = \frac{2}{e^{2\pi\Gamma_0 t}-1} \qquad \text{(S17)}$$

When the argument of the exponential is small (valid for $T \ll \mu \ll J$ and time t not too large) one can expand to leading order and find

$$T_{LL}(t_{\rm rm})^2 \sim= \frac{1}{\pi\Gamma_0 t}. \qquad \text{(S18)}$$

This gives a decay $T_{LL}(t_{\rm re}) \sim t^{-1/2}$ similar to the observation in Fig. 2 and S3. Interestingly this decay has the same power as the uncoupled SYK model, leading us to hypothesize that the SYK interactions are responsible for the $\Gamma_n \sim n$ broadening of the finite-frequency peaks.

This argument is supported by the revival oscillations in Fig. S3 (and Fig. 3 of the main text). Our first observation is that we reliably recover the expected two-point function decay of SYK, where $G_{\rm SYK}(t) \sim t^{-1/2}$. This behavior is reflected in the initial trend of the transmission amplitude T_{LL} up to times $t_{\rm gap} \sim 1/\mu^{2/3}$ where the wormhole physics in the form of revivals arise. For small enough μ and in the absence of "beating" in the revival oscillation, we can fit the decay of transmission amplitudes to a power law, $T_{LL,LR}(t = t_{\rm peak}) \sim t^{-\nu}$. The exponent ν is found to approach the characteristic value for the decay of correlation functions in SYK, $\nu \simeq \frac{1}{2}$.

This decay of revivals goes beyond the predictions of the dual gravity theory, and likely necessitates an additional mechanism beyond the low-energy conformal field theory discussion of Maldacena-Qi [S20]. A detailed analysis of the decay of revivals may provide valuable hints towards an extension of the low-energy theory [S20] to include non-conformal effects – e.g. to allow excitations to dissipate energy as they traverse the wormhole.

Symmetries of the Maldacena-Qi model

In this section we discuss useful symmetries of the MQ model. The most obvious is conservation of fermion parity, $P = (-1)^N \prod_{j=1}^N (\chi_L^j \chi_R^j)$, which is equivalent to fermion number (or charge) Q mod 2. This clearly commutes with the Hamiltonian (1) because the latter has only two-fermion and four-fermion terms. The MQ model also has a Z_4 symmetry defined as $q \equiv Q$ mod 4, which crucially relies on the perfectly correlated disorder between L and R SYK Hamiltonians in Eqs.(1)-(2) [S21].

The coupling term in the MQ Hamiltonian is proportional to the charge $Q = \sum_j c_j^\dagger c_j$. However it does not commute with the SYK terms (only Q mod 4 does). This is the main difference between the MQ and complex SYK models, the latter having $U(1)$ charge symmetry [S11].

We can also define a unitary operator U which takes $\chi_L^j \to \chi_L^j$ and $\chi_R^j \to -\chi_R^j$. This is a symmetry of the model with zero coupling ($\mu = 0$), and it anti-commutes with the charge operator, $\{Q, U\} = 0$. As a result the Z_4 sectors $q = 1, 3$, which are related by $Q \leftrightarrow -Q$, are mapped to each other by U and thus degenerate, $|n, 3\rangle = U|n, 1\rangle$ and vice versa. This will be useful in the following.

Analytical result for revivals at small coupling

To better understand the revival dynamics, it is helpful to look at the structure of the "single-Majorana" excita-

tions that we wish to transfer from one side to the other:

$$|j,L\rangle \equiv \chi_j^L|0\rangle \quad , \quad |j,R\rangle \equiv \chi_j^R|0\rangle \tag{S19}$$

Expanding in the eigenbasis of the Hamiltonian, we have

$$|j,\alpha\rangle = \sum_{n,q} c_j^\alpha(n,q)|n,q\rangle \tag{S20}$$

with $\alpha = L,R$. Here the sum is taken over all eigenstates $|n\rangle$ in the Z_4 "charge" sectors $q = 0,1,2,3$. The ground state $|0\rangle$ of the MQ model is always in the $q=0$ sector, therefore the excited states defined above are in one of the two odd-parity sectors, $q = 1,3$. The coefficients $c_j^\alpha(n,q)$ thus vanish for $q = 0,2$.

The (unaveraged) causal Green's functions $G^>_{LL}(t) = \langle 0|\chi_j^L(t)\chi_j^L|0\rangle$ and $G^>_{RL}(t) = \langle 0|\chi_j^R(t)\chi_j^L|0\rangle$ thus read

$$G^>_{LL}(t) = e^{iE_0 t}\sum_n \sum_{q=1,3} |c_j^L(n,q)|^2 e^{-iE_{n,q}t} \tag{S21}$$

$$G^>_{RL}(t) = e^{iE_0 t}\sum_n \sum_{q=1,3} \left(c_j^R(n,q)\right)^* c_j^L(n,q) e^{-iE_{n,q}t}$$

for a given, fixed mode j. Due to the all-to-all, random nature of the interactions within each flake, any choice of χ_j is equivalent on average. To understand the transmission of those "single-particle" excitations from one side of the wormhole to the other, we study the transmission $T^2_{\alpha L} = |G^>_{\alpha L}(t)|^2$. We have

$$T^2_{RL}(t) = \sum_{m,n}\sum_{p,q} \left[c_j^L(m,p)c_j^R(n,q)\right]^* c_j^L(n,q)c_j^R(m,p) \times e^{i(E_{m,p}-E_{n,q})t}, \tag{S22}$$

$$T^2_{LL}(t) = \sum_{m,n}\sum_{p,q} |c_j^L(m,p)|^2|c_j^L(n,q)|^2 e^{i(E_{m,p}-E_{n,q})t}. \tag{S23}$$

For the smallest system size $2N = 16$, and in the limit $\mu \ll \lambda \ll 1$, where λ is the typical finite-N level spacing, two dramatic simplifying features occur:

1) The spectrum in the odd sectors ($q = 1,3$) acquires the simple form

$$E_{m,1} = E_{m,3} + \omega_D. \tag{S24}$$

There is a *uniform* spectral shift between the two charge sectors. This is the mechanism at the root of the revival dynamics observed in ED (and the splitting of doublets observed in the spectral function). A simple calculation given below reveals why that uniform shift occurs.

2) The absolute value of the coefficients $c_j^\alpha(n,q)$ becomes *independent* of the charge sector q, and respect the following relation for all n:

$$c_j^L(n,1) = ic_j^R(n,1)\ ,\ c_j^L(n,3) = -ic_j^R(n,3) \tag{S25}$$

Combining these two features, we obtain the simple result

$$|G^>_{LL}(t)|^2 = 2\left(1+\cos\omega_D t\right)G_0(t)$$
$$|G^>_{RL}(t)|^2 = 2\left(1-\cos\omega_D t\right)G_0(t) \tag{S26}$$

where

$$G_0(t) = \sum_{m,n} |c_j(m)|^2|c_j(n)|^2 e^{i(E_{m,1}-E_{n,1})t} \tag{S27}$$

In this limit the behavior of the revival dynamics becomes clear: there is an envelope $\sim (1 \pm \cos\omega_D t)$ at a slow frequency set by the splitting between doublets, and fast oscillations at a large number of non-universal frequencies $E_{m,1} - E_{n,1}$ contained in $G_0(t)$, set by finite-size energy gaps characteristic of SYK physics. Considering only the non-oscillating part with $m = n$, we get

$$G_0(t) = \sum_m |c_j(m)|^4 \equiv R_j \tag{S28}$$

where we defined the participation ratio R_j of the initial excitation. This quantity characterizes the "inverse number of eigenstates" that are involved in the dynamics. This time-independent quantity sets the amplitude of the revivals,

$$|G^>_{LL/LR}(t)|^2 = 2\left(1 \pm \cos\omega_D t\right)R_j \tag{S29}$$

and it rapidly decreases with system size N, as shown in Fig. S4 c. This highlights the fact that the mechanism presented here cannot account for the revivals obtained in large-N solution – it relies crucially on the hierarchy of energy scales $\mu \ll \lambda \ll 1$.

Another way to understand this is to realize that Eq. (S27) corresponds to the Green's function of the canonical SYK model. As N increases, this quantity should approach the power-law decay $G_0(t) = |G_{\rm SYK}(t)|^2 \sim |t|^{-1}$. This decay occurs on a timescale J^{-1} much *smaller* than the revivals and will thus completely obscure them. What saves the day for small N is that the decay of $G_{\rm SYK}(t)$ is cut-off by finite-size effects at time $t \sim \lambda^{-1} \sim e^N/N$, which leaves room for revival oscillations at longer times, as seen in Fig. 4.

For larger N (such as $2N = 32$) the uniform splitting result, Eq. (S24) does not hold exactly – there is a weak dependence of the splitting frequency on the eigenstate index n. This gives rise to a decay in revivals, as observed in Fig. 4, because the doublets oscillate with a distribution of frequencies.

Perturbation theory

In the very weak coupling regime $\mu \ll \lambda$, one can utilize degenerate perturbation theory to gain some insight. As argued above, for $\mu = 0$ the spectrum of the model in identical in the charge sectors $q = 1,3$ due to the correlated disorder between the two SYK models. Introducing a non-zero μ couples each pair of degenerate states. To first-order we get a shift for U, Q (see also discussion of

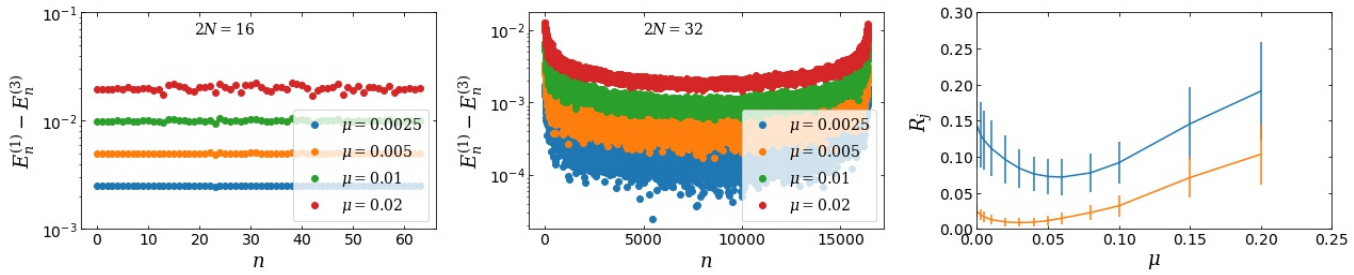

FIG. S4. Additional ED results. (a) and (b): Difference between the spectra in the different Z_4 symmetry sectors, $E_3 - E_1$, as a function of μ for $2N = 16$ (a) and $2N = 32$ (b). We observe a uniform spectral shift for $\mu \ll \lambda$ in (a) but not in (b). (c) Participation ratio of the excitation $\chi_j|0\rangle$ for various μ.

symmetries of the MQ model above)

$$E_{n,1} = \mu\langle n,1|Q|n,1\rangle \tag{S30}$$

$$\begin{aligned} E_{n,3} &= \mu\langle n,3|Q|n,3\rangle = \langle n,1|U^\dagger QU|n,1\rangle \\ &= -\langle n,1|Q|n,1\rangle = -E_{n,1} \end{aligned} \tag{S31}$$

which is *opposite* in the two Z_4 sectors. An additional result, valid for $2N = 16$ only, is that the expectation value

$$E_{n,1} = \mu\langle n,1|Q|n,1\rangle = \frac{\mu}{2} \tag{S32}$$

is independent of the eigenstate index n (see Fig. S4). This fixes $E_{m,1} = E_{m,3} + \omega_D$ above with $\omega_D = \mu$. However, we have not yet been able to find a solid argument to explain the statement of Eq. (S32).